Three-dimensional lattice Boltzmann model for magnetic reconnection

M. Mendoza* and J. D. Muñoz†

Simulation of Physical Systems Group, Universidad Nacional de Colombia, Departamento de Fisica, Crr 30 # 45-03, Ed. 404, Of. 348, Bogotá D.C., Colombia

(Received 23 April 2007; published 29 February 2008)

We develop a three-dimensional (3D) lattice Boltzmann model that recovers in the continuous limit the two-fluids theory for plasmas, and consequently includes the generalized Ohm's law. The model reproduces the magnetic reconnection process just by giving the right initial equilibrium conditions in the magnetotail, without any assumption on the resistivity in the diffusive region. In this model, the plasma is handled similar to two fluids with an interaction term, each one with distribution functions associated to a cubic lattice with 19 velocities (D3Q19). The electromagnetic fields are considered as a third fluid with an external force on a cubic lattice with 13 velocities (D3Q13). The model can simulate either viscous fluids in the incompressible limit or nonviscous compressible fluids, and successfully reproduces both the Hartmann flow and the magnetic reconnection in the magnetotail. The reconnection rate in the magnetotail obtained with this model lies between $R=0.062$ and $R=0.073$, in good agreement with the observations.

DOI: 10.1103/PhysRevE.77.026713 PACS number(s): 47.11.−j, 94.30.cp, 52.30.Ex, 52.65.−y

I. INTRODUCTION

The magnetic reconnection is one of the most interesting phenomenon of plasma physics. This process quickly transforms the magnetic energy into termic and kinetic energies of the plasma. It is mostly observed inside of astrophysical plasmas, such as solar flares (where it contributes to the plasma heating), and in the terrestrial magnetosphere, where it support the income flux of plasma and electromagnetic energy.

The magnetic reconnection requires the existence of a diffusive region, where dissipative electric fields change the magnetic field topology. The first models were independently formulated by Sweet [1] in 1958 and Parker [2] in 1957. They suggested that the magnetic reconnection is a steady-state resistive process that occurs in the vicinity of a neutral line. This model reduces the phenomenon to a boundary condition problem and can explain the magnetic field reconnection. However, it has some problems when compared with experimental observations (i.e., a very slow reconnection rate), and it leaves unexplained the origin of the high-resistive region. In 1964, Petschek [3] proposed the first model for fast reconnection rates. He included a much smaller diffusion region than the Sweet-Parker model, but he suggested that the rest of the boundary layer region should consist of slow shock waves that accelerate the plasma up to the Alfven velocity. Nevertheless, the origin of the diffusive region remains unexplained.

At present, the nature of this phenomenon has been studied by using kinetic theory and considering collisionless plasmas, since this is a common property of astrophysical plasmas. One of the developments of the kinetic theory is the generalized Ohm's law, where some extra terms explain the existence of a dissipative electric field. The introduction of these extra terms in resistive magnetohydrodynamics is called MHD Hall [4]. A useful approximation of the kinetic theory consists of modeling the plasma similar to two fluids (one electronic and one ionic), which have independent momentum, mass conservation, and state equations, plus an interaction term in the momentum equation [4]. This treatment, in the one-fluid limit, introduces in a natural way the extra terms of the generalized Ohm's law. However, the equations involved by this treatment are complex and it is difficult to find an analytic solution for any problem.

For this reason, most plasma processes are studied by numerical methods. One of the numerical methods for simulating fluids is lattice Boltzmann (LB) [5], which was developed from lattice-gas automata. Lattice Boltzmann simulations are performed on regular grids of many cells and a small number of velocity vectors per cell, each one associated to a density distribution function, which evolve and spread together to the neighbor cells according to the collisional Boltzmann equation. The first LB model for studying plasmas reproduces the resistive magnetohydrodynamic equations and was developed by Chen and co-workers [6,7] as an extension of the lattice-gas model developed by Chen and Matthaeus [8] and Chen, Matthaeus, and Klein [9]. This LB model uses 37 velocity vectors per cell on a square lattice and is developed for two dimensions. Thereafter, Martinez, Chen, and Matthaeus [10] decreased the number of velocity vectors from 37 to 13, which made easier a future three-dimensional (3D) extension. Some of the first LB models for magnetohydrodynamics in 3D was developed by Osborn [11] and Breyiannis and Valougeorgi [12]. They used 19 vectors on a cubic lattice for the fluid, plus 7 vectors for the magnetic field, which makes a total number of 26 vectors per cell. By following a different path, Fogaccia, Benzi and Romanelli [13] introduced a 3D LB model for simulating turbulent plasmas in the electrostatic limit. All these models reproduce the resistive magnetohydrodynamic equations for a single fluid.

In this paper, we introduce a 3D lattice Boltzmann model that recovers the plasma equations in the two-fluids theory. In this way, the model is able to reproduce magnetic reconnection, without the *a priori* introduction of a resistive re-

*mmendozaj@unal.edu.co
†jdmunozc@unal.edu.co

gion. Moreover, it is able to reproduce the fluid state equation with a general polytropic coefficient. The model uses 39 vectors per cell and 63 probability density functions (19 for each fluid, 25 for the electrical and magnetic fields). In Sec. II we describe the model with the evolution rules and the equilibrium expressions involved for the 63 density functions, plus the way to compute the electric, magnetic, and velocity fields. The Chapman-Enskog expansion showing how these rules recover the two-fluids magnetohydrodynamic equations is developed in the Appendix. In order to validate the model, we simulate the 2D Hartmann's flow in Sec. III, and, finally, the magnetic reconnection for a magnetotail equilibrium configuration in Sec. IV. The main results and conclusions are summarized in Sec. V.

II. 3D LATTICE BOLTZMANN MODEL FOR A TWO-FLUIDS PLASMA

In a simple lattice Boltzmann model [5], the D-dimensional space is divided into a regular grid of cells. Each cell has Q vectors $\vec{v}_i$ that links itself with its neighbors, and each vector is associated to a distribution function f_i. The distribution function evolves according to the Boltzmann equation,

$$f_i(\vec{x}+\vec{v}_i,t+1)-f_i(\vec{x},t)=\Omega_i(\vec{x},t), \tag{1}$$

where $\Omega_i(\vec{x},t)$ is a collision term, which is usually taken as a time relaxation to some equilibrium density, f_i^{eq}. This is known as the Bhatnagar-Gross-Krook (BGK) operator [14],

$$\Omega_i(\vec{x},t)=-\frac{1}{\tau}[f_i(\vec{x},t)-f_i^{\mathrm{eq}}(\vec{x},t)], \tag{2}$$

where τ is the relaxation time and $f_i^{\mathrm{eq}}(\vec{x},t)$ is the equilibrium function. The equilibrium function is chosen in such a way that (in the continuum limit) the model simulates the actual physics of the system.

For our 3D model, we use a cubic regular grid, with lattice constant $\delta x=\sqrt{2}c\delta t$ and c is the light speed ($c\simeq 3\times 10^8$ m/s). In other words, $c=1/\sqrt{2}$ in normalized lattice units (time unit $=\delta t$, spatial unit $=\delta x$). There are 19 velocity vectors for the electronic and ionic fluids (Fig. 1), 13 different vectors for the electric field (Fig. 2), and 7 different vectors for the magnetic field (Fig. 3). The velocity vectors are denoted by $\vec{v}_i^p$, where $i=1,2,3,4,5,6$ indicates the direction and $p=0,1,2$ indicates the plane of location (Fig. 1). Twelve of them ($i=1,2,3,4$) have magnitude $\sqrt{2}$, in lattice units, and lie on the diagonals of the planes. Their components are

$$\vec{v}_i^0=\sqrt{2}\{\cos[(2i-1)\pi/4],\sin[(2i-1)\pi/4],0\}, \tag{3a}$$

$$\vec{v}_i^1=\sqrt{2}\{\cos[(2i-1)\pi/4],0,\sin[(2i-1)\pi/4]\}, \tag{3b}$$

$$\vec{v}_i^2=\sqrt{2}\{0,\cos[(2i-1)\pi/4],\sin[(2i-1)\pi/4]\}. \tag{3c}$$

Six velocity vectors ($i=5,6$) have magnitude 1 and point to the centers of the cube faces in Fig. 1. Their components are

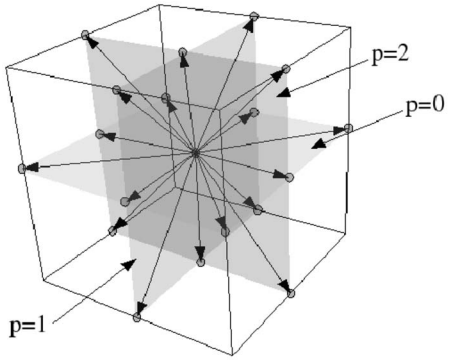

FIG. 1. The distribution functions associated to a cubic lattice with 19 velocities (D3Q19) modeling the electronic and ionic fluids. The arrows represent the velocity vectors $\vec{v}_i^p$ and p indicates the plane of location.

$$\vec{v}_i^0=((-1)^i,0,0), \tag{4a}$$

$$\vec{v}_i^1=(0,(-1)^i,0), \tag{4b}$$

$$\vec{v}_i^2=(0,0,(-1)^i). \tag{4c}$$

This makes 18 vectors. The missing one is the rest vector $\vec{v}_0$, with components $(0,0,0)$.

Associated to each velocity vector $\vec{v}_i^p$ of magnitude $\sqrt{2}$ [$i=1,2,3,4$, Eq. (3)] are two electric vectors $\vec{e}_{ij}^p$ and two magnetic vectors $\vec{b}_{ij}^p$ ($j=0,1$), which are used to compute the electromagnetic fields (Fig. 4). The electric vectors are perpendicular to $\vec{v}_i^p$ and lie on the same plane p. The magnetic vectors are perpendicular to $\vec{v}_i^p$, too, but they are also perpendicular to the plane p. In terms of the velocity vectors (3), they are

$$\vec{e}_{i0}^p=\frac{1}{2}\vec{v}_{[(i+2) \bmod 4]+1}^p, \quad \vec{e}_{i1}^p=\frac{1}{2}\vec{v}_{[i \bmod 4]+1}^p, \tag{5}$$

with the rest vector $\vec{e}_0=(0,0,0)$, and

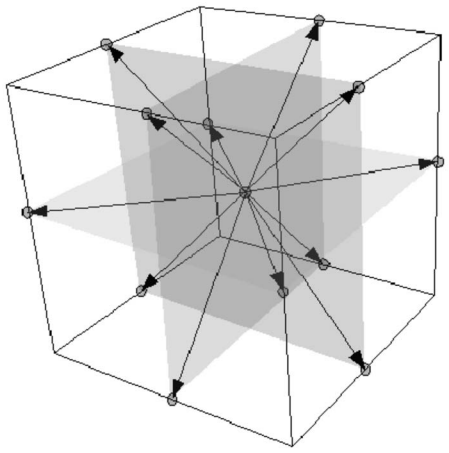

FIG. 2. Cubic lattice D3Q13 for modeling the electric field. The arrows represent the electric vectors $\vec{e}_{ij}^p$.

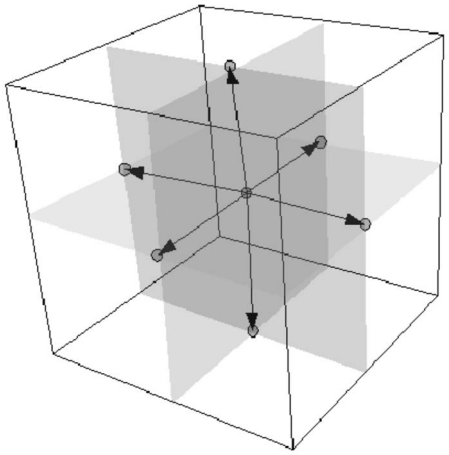

FIG. 3. Cubic lattice D3Q7 for simulating the magnetic field, the arrows indicate the magnetic vectors $\vec{b}_{ij}^{p}$.

$$\vec{b}_{ij}^{p} = \vec{v}_{i}^{p} \times \vec{e}_{ij}^{p}, \tag{6}$$

with the rest vector $\vec{b}_0=(0,0,0)$. With these definitions, there are 25 electric field vectors, but only 13 of them are different. Similarly, there are 25 magnetic field vectors, but only 7 are different.

The velocity and density fields for both electrons and ions plus the electromagnetic fields are computed from distribution functions that propagate from cell to cell with the velocity vectors $\vec{v}_i^p$. For each fluid (electrons or ions) there is a distribution function associated with each velocity vector, that is 19+19=38 functions for the fluids. They are denoted by $f_i^{p(s)}$ and $f_0^{(s)}$, propagating with the velocity vectors $\vec{v}_i^p$ and $\vec{v}_0$, respectively. Hereby, the index s distinguishes between electronic ($s=0$) and ionic ($s=1$) fluids. For the electromagnetic fields there are two distribution functions associated with each velocity vector of magnitude $\sqrt{2}$, denoted by G_{ij}^p ($j=0,1$), plus a single function associated with the rest vector $\vec{v}_0$, denoted by G_0, that is $2\times 12+1=25$ distribution functions for the electromagnetic fields. This gives a total number of 63 distribution functions per cell. The macroscopic variables are computed from them as follows:

$$\rho_s = f_0^s + \sum_{i=1}^{6}\sum_{p=0}^{2} f_i^{p(s)}, \tag{7a}$$

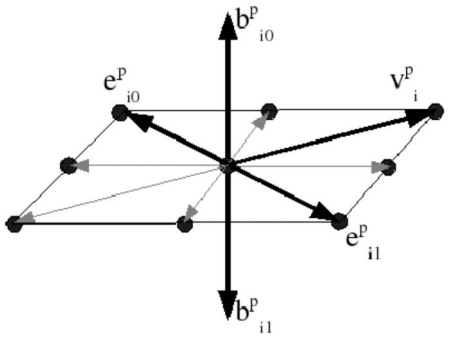

FIG. 4. Index relationship between the velocity vectors and the electric and magnetic vectors.

$$\rho_s \vec{V}_s = \sum_{i=1}^{6}\sum_{p=0}^{2} f_i^{p(s)} \vec{v}_i^{p}, \tag{7b}$$

$$\vec{E} = \sum_{i=1}^{4}\sum_{p=0}^{2}\sum_{j=0}^{1} G_{ij}^{p} \vec{e}_{ij}^{p}, \tag{7c}$$

$$\vec{B} = \sum_{i=1}^{4}\sum_{p=0}^{2}\sum_{j=0}^{1} G_{ij}^{p} \vec{b}_{ij}^{p}, \tag{7d}$$

$$\vec{J} = \sum_{s=0}^{1} \frac{q_s}{m_s} \rho_s \vec{V}_s, \tag{7e}$$

$$\rho_c = \sum_{s=0}^{1} \frac{q_s}{m_s}, \tag{7f}$$

where ρ_s is the density of each fluid, $\vec{V}_s$ is a subsidiary field that represent the velocity of each fluid before including external forcements (i.e., before the collision [15]), and m_s and q_s are its particle mass and charge (here, $s=0$ represents electrons and $s=1$ represents ions, as before). In addition, $\vec{E}$ and $\vec{J}$ are subsidiary fields that represent the electric field and the total current density before external forcements, $\vec{B}$ is the magnetic field, and ρ_c is the total charge density.

For the evolution of these distribution functions we follow the proposal of Guo *et al.* [15] which includes external forcements in the lattice Boltzmann equations as follows:

$$f_i^{p(s)}(\vec{x}+\vec{v}_i^p, t+1) - f_i^{p(s)}(\vec{x},t) = \Omega_i^{p(s)}(\vec{x},t) + T_i^{(s)}, \tag{8}$$

$$G_{ij}^{p}(\vec{x}+\vec{v}_i^p, t+1) - G_{ij}^{p}(\vec{x},t) = \Omega_{ij}^{p(2)}(\vec{x},t) + T_i^{(2)}, \tag{9}$$

$$f_0^{(s)}(\vec{x}, t+1) - f_0^{(s)}(\vec{x},t) = \Omega_0^{(s)}(\vec{x},t) + T_0^{(s)}, \tag{10}$$

$$G_0(\vec{x}, t+1) - G_0(\vec{x},t) = \Omega_0^{(2)}(\vec{x},t) + T_0^{(2)}, \tag{11}$$

where $T_i^{(K)}$ and $T_0^{(K)}$ are forcement coefficients ($K=0,1,2$), defined by [15]

$$T_i^{(s)} = \left(1 - \frac{1}{2\tau_s}\right) w_i \left[3(\vec{v}_i^p - \vec{V}_s') \cdot \vec{F}^{(s)} + 9(\vec{v}_i^p \cdot \vec{V}_s')(\vec{v}_i^p \cdot \vec{F}_s)\right], \tag{12a}$$

$$T_0^{(s)} = \left(1 - \frac{1}{2\tau_s}\right) w_0 \left[-3(\vec{V}_s' \cdot \vec{F}^{(s)})\right], \tag{12b}$$

$$T_i^{(2)} = 0, \tag{12c}$$

$$T_0^{(2)} = 0. \tag{12d}$$

The weights w_i are $w_0=\frac{1}{3}$, $w_{1,2,3,4}=\frac{1}{36}$, $w_{5,6}=\frac{1}{18}$, and τ_K are relaxation times. The force vectors $\vec{F}^{(s)}$ in Eq. (12) are

$$\vec{F}^{(s)} = \frac{q_s}{m_s}\rho_s(\vec{E}' + \vec{V}_s \times \vec{B}) - \nu\rho_s(\vec{V}_s - \vec{V}_{(s+1) \bmod 2}) + \vec{F}_0^{(s)}, \tag{13}$$

where

$$\vec{E}' = \vec{E} - \frac{1}{4}\mu_0\vec{J}', \tag{14}$$

is the mean electric field, ν is the collision frequency of the plasma, and $\vec{F}_0^{(s)}$ is any external force (for instance, a gravitational force). The mean density current vector $\vec{J}'$ in Eq. (14) includes these forcements and is defined by

$$\vec{J}' = \vec{J} + \sum_s \frac{q_s}{m_s}\left(\frac{1}{2}\vec{F}^{(s)}\right). \tag{15}$$

In addition, the mean velocity vector $\vec{V}'_s$ is defined by [15]

$$\vec{V}'_s = \vec{V}_s + \frac{\vec{F}^{(s)}}{2\rho_s}. \tag{16}$$

In order to have the force vectors $\vec{F}^{(s)}$ in terms of the subsidiary fields, we replace Eq. (15) into Eq. (14) to obtain

$$\vec{E}' = \vec{E} - \frac{1}{4}\mu_0\left[\vec{J} + \sum_s \frac{q_s}{m_s}\left(\frac{1}{2}\vec{F}^{(s)}\right)\right], \tag{17}$$

and we solve the set of equations, Eqs. (13) and (17), with the following result:

$$\vec{F}^{(0)} = \frac{\left[1 + \frac{q_1^2}{8m_1^2}\mu_0\rho_1\right]\vec{Z}^{(0)}}{1 + \frac{1}{8}\mu_0\left[\frac{q_0^2}{m_0^2}\rho_0 + \frac{q_1^2}{m_1^2}\rho_1\right]} - \frac{\left[\frac{q_1 q_0}{8m_1 m_0}\mu_0\rho_0\right]\vec{Z}^{(1)}}{1 + \frac{1}{8}\mu_0\left[\frac{q_0^2}{m_0^2}\rho_0 + \frac{q_1^2}{m_1^2}\rho_1\right]}, \tag{18a}$$

$$\vec{F}^{(1)} = \frac{\left[1 + \frac{q_0^2}{8m_0^2}\mu_0\rho_0\right]\vec{Z}^{(1)}}{1 + \frac{1}{8}\mu_0\left[\frac{q_0^2}{m_0^2}\rho_0 + \frac{q_1^2}{m_1^2}\rho_1\right]} - \frac{\left[\frac{q_1 q_0}{8m_1 m_0}\mu_0\rho_1\right]\vec{Z}^{(0)}}{1 + \frac{1}{8}\mu_0\left[\frac{q_0^2}{m_0^2}\rho_0 + \frac{q_1^2}{m_1^2}\rho_1\right]}, \tag{18b}$$

where the vectors $\vec{Z}^{(s)}$ are defined by

$$\vec{Z}^{(s)} = \frac{q_s}{m_s}\rho_s\left(\vec{E} - \frac{1}{4}\mu_0\vec{J} + \vec{V}_s \times \vec{B}\right) - \nu\rho_s(\vec{V}_s - \vec{V}_{(s+1) \bmod 2}) + \vec{F}_0^{(s)}. \tag{19}$$

Next, we adopt BGK collision terms $\Omega_{ij}^{p(K)}$ and $\Omega_0^{(K)}$ of the form [14]

$$\Omega_i^{p(s)} = -\frac{1}{\tau_s}[f_i^{p(s)}(\vec{x},t) - f_i^{p(s)\mathrm{eq}}(\vec{x},t)], \tag{20a}$$

$$\Omega_{ij}^{p(2)} = -\frac{1}{\tau_2}[G_{ij}^{p}(\vec{x},t) - G_{ij}^{p\mathrm{eq}}(\vec{x},t)], \tag{20b}$$

$$\Omega_0^{(s)} = -\frac{1}{\tau_s}[f_0^{(s)}(\vec{x},t) - f_0^{(s)\mathrm{eq}}(\vec{x},t)], \tag{20c}$$

$$\Omega_0^{(2)} = -\frac{1}{\tau_2}[G_0(\vec{x},t) - G_0^{\mathrm{eq}}(\vec{x},t)]. \tag{20d}$$

The equilibrium functions for the fluids $f_i^{p(s)\mathrm{eq}}$ and $f_0^{(s)\mathrm{eq}}$ are

$$f_i^{p(s)\mathrm{eq}}(\vec{x},t) = \omega_i\rho_s\left[3\xi_s\rho_s^{\gamma-1} + 3(\vec{v}_i^{\,p}\cdot\vec{V}'_s) + \frac{9}{2}(\vec{v}_i^{\,p}\cdot\vec{V}'_s)^2 - \frac{3}{2}(\vec{V}'^{\,2}_s)\right], \tag{21a}$$

$$f_0^{p(s)\mathrm{eq}}(\vec{x},t) = 3\rho_s\left[1 - \frac{1}{2}(4\xi_s\rho_s^{\gamma-1} + \vec{V}'^{\,2}_s)\right]. \tag{21b}$$

Hereby, ξ_s is a constant that is fixed by the state equation for the plasma as follows. We assume for the plasma a state equation of the form

$$P_s = \left(\frac{\rho_{(s)0}}{\rho_s}\right)^{\gamma} P_{(s)0}, \tag{22}$$

where γ is the polytropic index and $P_{(s)0}$ and $\rho_{(s)0}$ are the characteristic fluid pressure and density. For all purposes, the pressure is computed from the density via this equation. Then, the constant ξ_s is defined as

$$\xi_s = P_{(s)0}\rho_{(s)0}^{-\gamma}. \tag{23}$$

For the electromagnetic field $(K=2)$ we have

$$G_{ij}^{p\ \mathrm{eq}}(\vec{x},t) = \frac{1}{4}\vec{E}'\cdot\vec{e}_{ij}^{\,p} + \frac{1}{8}\vec{B}\cdot\vec{b}_{ij}^{\,p}, \tag{24a}$$

$$G_0^{\mathrm{eq}}(\vec{x},t) = 0. \tag{24b}$$

This completes the definition of the lattice Boltzmann.

The proof that this lattice Boltzmann model, via a Chapman-Enskog expansion, recovers the equations of the two-fluids theory for a plasma composed by electrons and ions is shown in the Appendix . The model lets us consider either compressible and nonviscous fluids or incompressible and viscous fluids. The first ones are governed by the continuity equation

$$\vec{\nabla}\cdot(\rho_s\vec{V}'_s) + \frac{\partial\rho_s}{\partial t} = 0, \tag{25}$$

the Navier-Stokes equation (up to second order in ϵ)

$$\rho_s\left(\frac{\partial\vec{V}'_S}{\partial t} + (\vec{V}'\cdot\vec{\nabla})\vec{V}'_s\right) = -\vec{\nabla}P_s + \frac{q_s}{m_s}\rho_s(\vec{E} + \vec{V}'_s \times \vec{B}) - \nu\rho_s(\vec{V}'_s - \vec{V}'_{(s+1) \bmod 2}) + \vec{F}_0, \tag{26}$$

the state equation

$$P_s = \xi_s \rho_s^{\gamma} \tag{27}$$

(with P_s the fluid pressure), and the Maxwell equations. The second ones are governed by the state equation (27), the Maxwell equations, the continuity equation

$$\vec{\nabla} \cdot \vec{V}'_s = 0, \tag{28}$$

and the Navier-Stokes equation for an incompressible and viscous fluid (up to second order in ϵ),

$$\rho_s \left(\frac{\partial \vec{V}'_s}{\partial t} + (\vec{V}' \cdot \vec{\nabla}) \vec{V}'_s \right) = -\vec{\nabla} P_s + \frac{q_s}{m_s} \rho_s (\vec{E} + \vec{V}'_s \times \vec{B}) - \nu \rho_s (\vec{V}'_s - \vec{V}'_{(s+1) \bmod 2}) + \vec{F}_0 + \eta_s \rho_s \vec{\nabla}^2 \vec{V}'_s, \tag{29}$$

with kinematic viscosity $\eta_s = \frac{1}{3}(\tau_s - 1/2)$.

III. SIMULATION OF A 2D HARTMANN FLOW

In the MHD limit, the two-fluid theory becomes the MHD (one fluid) theory, which is represented by the following equations: the continuity of mass,

$$\vec{\nabla} \cdot (\rho \vec{V}) + \frac{\partial \rho}{\partial t} = 0, \tag{30}$$

the Navier-Stokes equation,

$$\rho \left(\frac{\partial}{\partial t} + \vec{V} \cdot \vec{\nabla} \right) \vec{V} = -\vec{\nabla} P + \vec{J} \times \vec{B} + \eta \vec{\nabla}^2 \vec{V} + \vec{F}_0, \tag{31}$$

the magnetic field equation,

$$\frac{\partial \vec{B}}{\partial t} = \vec{\nabla} \times (\vec{V} \times \vec{B}) + \eta_m \vec{\nabla}^2 \vec{B}, \tag{32}$$

and the state equation,

$$P = \xi_s \rho^{\gamma}, \tag{33}$$

where ρ is the total mass density, $\vec{V}$ is the total velocity field, and $\eta_m = \frac{1}{\mu_0 \sigma_0}$ is the magnetic viscosity.

For the Hartmann flow [12,16,17], we consider a fluid in isotermal equilibrium ($\gamma = 1$) at low temperature (a small ξ_s value), incompressible and viscous. The fluid moves in the x direction between two walls at rest at $y = -L$ and $y = -L$. There is a constant magnetic field in the y direction, with intensity B_0, and a constant external force $F = \rho g$ in the x direction that drags the fluid [16]. So, the velocity and magnetic fields take the forms $\vec{V} = (V_x(y), 0, 0)$ and $\vec{B} = (B_x(y), B_0, 0)$, respectively. By replacing these expressions in Eqs. (31) and (32), one finds the following solutions for the velocity and magnetic fields [16]:

$$V_x(y) = \sqrt{\frac{\rho \eta_m}{\eta}} \frac{gL}{B_0} \cosh H \left(1 - \frac{\cosh(Hy/L)}{\cosh(H)} \right), \tag{34a}$$

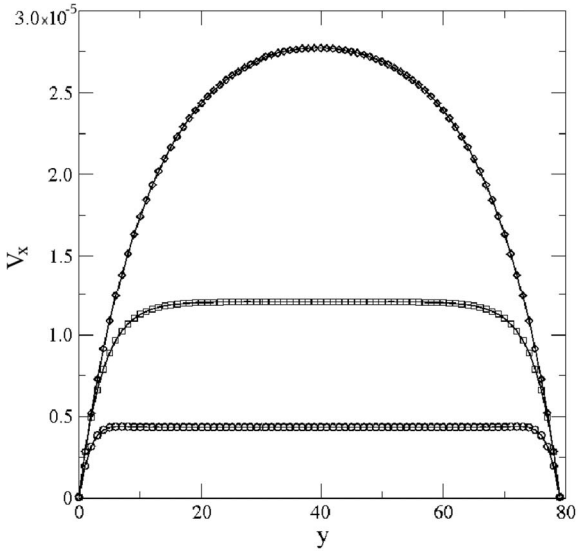

FIG. 5. Velocity profile V_x vs y for different Hartmann numbers: $H = 6.0$ (diamonds), $H = 13.0$ (squares), and $H = 26.0$ (circles). The solid lines are the analytical results.

$$B_x(y) = \frac{\rho g L}{B_0} \left[\frac{\sinh(Hy/L)}{\sinh(H)} - \frac{y}{L} \right], \tag{34b}$$

where $H = \frac{B_0 L}{\sqrt{\rho \eta \eta_m}}$ is the Hartmann number and $-L \le y \le L$.

For the simulation, we use a single row of 80 cells in the y direction, with periodic boundary conditions in both x and z directions. The initial conditions for the density functions are obtained from the equilibrium expressions (21) and (24) with the values $\vec{V}_s = 0$, $\rho_s = m_s n_s$, $\vec{E} = 0$, $\vec{B} = (0, B_0, 0)$, and $\vec{F}_0^{(s)} = (\rho_s g, 0, 0)$. In addition, the constant values are $\gamma = 1$, $\xi_s = 3 \times 10^{-6}$, $\mu_0 = 1.0$, $\nu = 100$, $\tau_s = 1.0$, $\tau_2 = 0.5$, $m_0 = 1.0 \times 10^{-19}$, $m_1 = 1820 m_0$, and $n_0 = n_1 = 1.0 \times 10^{23}$ particles per unit volume. For the y direction, we assume as boundary conditions at the walls that the equilibrium density functions for the time evolution [Eqs. (21) and (24)] are always the same from the initial conditions (including $\vec{V}_s = 0$, i.e., nonconducting walls). The system evolves until a steady state is reached. We ran simulations for Hartmann numbers $H = 6.0$, 13.0, and 26.0, and the magnetic field B_0 was chosen to obtain these Hartmann numbers.

Figure 5 shows the velocity profiles and Fig. 6 shows the magnetic field profiles for the three cases. The solid lines are the analytic solutions [Eq. (34)]. The simulation results are in excellent agreement with the analytical solutions. This result shows that (at least for the MHD limit) our LB model works properly.

IV. APPLICATION TO MAGNETIC RECONNECTION

A. Dynamics of the magnetic reconnection process

In order to simulate the magnetic reconnection in the magnetotail, we chose the initial equilibrium condition proposed by Harris [18,19] for the current sheet, plus a magnetic dipole field, orthogonal to the sheet. For this simulation we assume that the fluids are nonviscous and compressible.

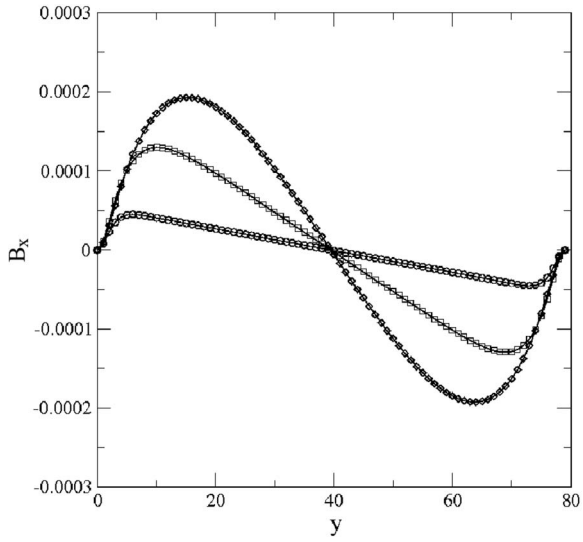

FIG. 6. Magnetic field intensity B_x vs y for different Hartmann numbers: $H=6.0$ (diamonds), $H=13.0$ (squares), and $H=26.0$ (circles). The solid lines are the analytical results.

The current sheet lies on the x-y plane, and its magnetic field is described by the vector potential $\vec{A}=(0,A_y,0)$ with

$$A_y(x,z) = LB_0 \ln \cosh[v(x)(z/L)]/v(x), \tag{35}$$

where the effective thickness of the current sheet is given by $L/v(x)$, and the asymptotic strength, B_0, is the value of B_x in the limit $z\to\infty$, divided by $v(x)$. The function $v(x)$ is an arbitrary slowly varying function. We choose for $v(x)$ the quasiparabolic function proposed by [20,21]

$$v(x) = \exp(-\epsilon x/L), \tag{36}$$

where the parameter ϵ is much smaller than one and determines the strength of the z component of the magnetic field. We took $\epsilon=0.1$ for the simulation. The initial density is the one proposed by Harris,

$$n_s(x,z) = n_b + n_c v^2(x)\cosh^{-2}[v(x)(z/L)], \tag{37}$$

where n_b is the background density and n_b+n_c is the maximal density.

The magnetic dipole is set at position x_0 with momentum M and oriented in the z direction. It generates a magnetic field given by

$$B_x(x,z) = \frac{3M(x-x_0)z}{[(x-x_0)^2+z^2]^{5/2}},$$

$$B_y(x,z) = 0,$$

$$B_z(x,z) = \frac{M[2z^2-(x-x_0)^2]}{[(x-x_0)^2+z^2]^{5/2}}. \tag{38}$$

The lattice constant δx is chosen as one seventh of the ion inertial length, $\delta x=\frac{1}{7}c/\omega_1$, where ω_1 is the ion plasma frequency, $\omega_1=\sqrt{\frac{q_1^2 n_1}{\epsilon_0 m_1}}$, with $n_1=10^5$ particles per cubic meter for the magnetotail [22] and m_1 the proton mass. That gives $\delta x \simeq 103$ km. Since the current sheet in the magnetotail can be assumed around 3000 km width [22,23], we chose $L=2c/\omega_1$. For the position of the magnetic dipole, we took $x_0=22.7c/\omega_1$ and for the dipole momentum, $M=3\times10^{12}$. The grid is an array of 100×100 cells on the x-z plane with periodic boundary conditions in the y direction and free boundary conditions for the fields in the other directions (each boundary cell copies the density functions of its first neighbor in ortogonal direction to the boundary at each time step). Thus, the simulation region is a square of $14.26c/\omega_1$ length (around 10 300 km). For this simulation we took $m_0=m_1/100$ (i.e., an electron mass 20 times larger than the real one) in order to obtain numerical stability, but it has been shown [24] that this point does not qualitatively change the physical results. The temperature ratio is chosen to be $T_0/T_1=0.2$, according to observational results [25]. For this simulation, we took $n_c=5n_b$ and $n_b=0.17n_1$. Figures 7–10 show the evolution of the magnetic field lines in the magnetic reconnection process. This appears in a natural way, without the *a priori* introduction of any resistive region. The factor Ω_1 is the ionic cyclotron frequency, $\Omega_1=q_1B_0/m_1$. This result shows that the model can actually simulate the magnetic reconnection. This simulation took 1 h in a Pentium IV PC of 2.8 GHz, i.e., it is fast.

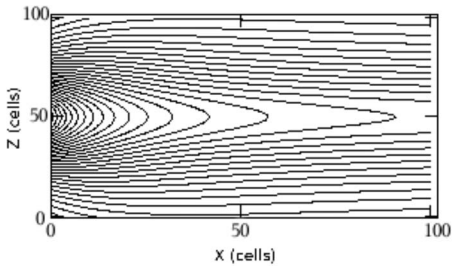

FIG. 7. Magnetic field lines in the magnetic reconnection process at $t=0$ (initial conditions).

B. Reconnection rates

To compute real reconnection rates we performed a similar simulation to the one before, but with the actual ratio between electronic and ionic masses ($m_1=1820m_0$). This choice makes us choose shorter time steps ($\delta t=3.54\times10^{-5}$ s) and smaller cells ($\delta x=15$ km) in order to reproduce with accuracy the electron moves. The simulation region is of 1500 km in x and 1500 km in z. Since the region is smaller than before, $v(x)=1$ is a good approximation on the

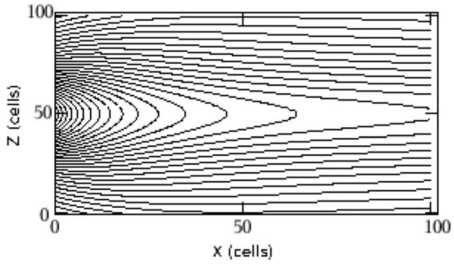

FIG. 8. Evolution for the magnetic field lines in the magnetic reconnection process at $t=3/\Omega_1$.

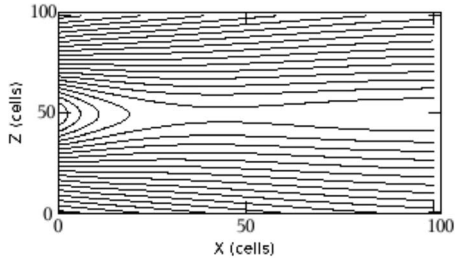

FIG. 9. Evolution for the magnetic field lines in the magnetic reconnection process at $t=15/\Omega_1$.

entire region. The resolution of the grid was 100×100, but the entire simulation was repeated with a second resolution of 200×200, without finding any notorious differences. The simulation constants are $L=1500$ km [22] and $B_0=10.0$ nT [23]. The electronic temperature is chosen as $T_0=5.8$ MK and the ionic one as $T_1=23.2$ MK [25]. All these are observational data. The electronic mass is taken $m_0=9.11\times10^{-31}$ kg and the ionic mass is $m_1=1.67\times10^{-27}$ kg. Because the initial equilibrium condition, proposed by Harris [18,19] for the current sheet, is based on resistive MHD and our simulation is based on two-fluids theory, we take a different initial condition, with initial densities in Eq. (37) as $n_c=0$ and $n_b=10^5$ m^{-3}. All other constants of our LB model take their standard values in the International System of Units units.

This initial configuration is not in equilibrium. For this reason, our simulation has two parts. In the first one, we impose the current sheet configuration, and fields and fluids are allown to change according to the two-fluids theory until reaching an equilibrium condition. In the second one, the system starts from that equilibrium condition and evolves without any imposition, i.e., this is the actual phenomenon we want to study.

The first part of the simulation took $5000\delta t$ and the equilibrium configuration we obtained for the magnetic field is shown in Fig. 11. The same field after 2500 more steps, i.e., in the second part, is drawn in Fig. 12, showing a reconnection. To calculate the reconnection rate, we use the definition

$$R=\frac{V_{in}}{V_A}, \tag{39}$$

where V_{in} is the inflow velocity of the plasma to the diffusive zone, and V_A is the characteristic Alfvén velocity.

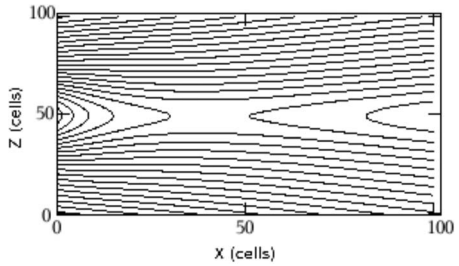

FIG. 10. Evolution for the magnetic field lines in the magnetic reconnection process at $t=20/\Omega_1$.

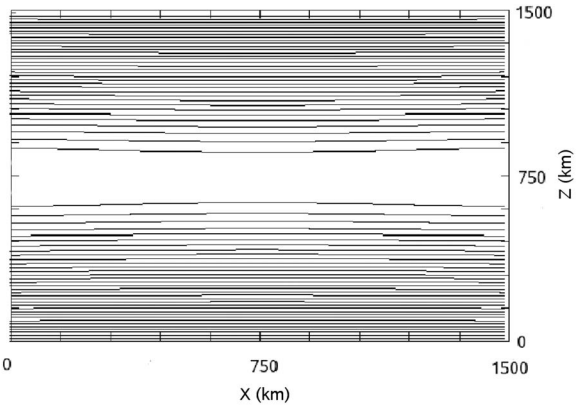

FIG. 11. Magnetic field lines in the magnetic reconnection process at $t=5000\delta t$ (equilibrium conditions).

The Alfvén velocity is defined by

$$V_A=\frac{B'}{\sqrt{\mu_0 n_b(m_1+m_0)}}, \tag{40}$$

where B' is the magnetic field intensity.

Our model, in contrast with other ones, does not include an explicit diffusive zone, but we can see the expected asymptotic behavior of the inflow and Alfven velocities for a reconnection region (Fig. 13). The asymptotic limits, however, change if one takes a larger simulation space. Thus, we have opted for defining a reconnection rate for each value of the z coordinate across the current sheet by computing the Alfvén velocity as a function of z and dividing the plasma inflow velocity at each z by the Alfvén velocity there (Fig. 14). By this way, we obtain reconnection rates for this central region between 0.062 and 0.073, which are in good agreement with the experimental observations of around $R\sim0.1$ [26]. The shape of the curve changes if one takes a smaller simulation space, but the peaks lay more or less in the same range. Nevertheless, this is not a numerical instability. Indeed, if we run the same simulation with a finer grid (200×200 cells of 7.5 km size), we obtain the same curves as before. This simulation with 100×100 cells of 15 km size took just 6 hours in a Pentium IV PC of 32 bits at 3.0 GHz.

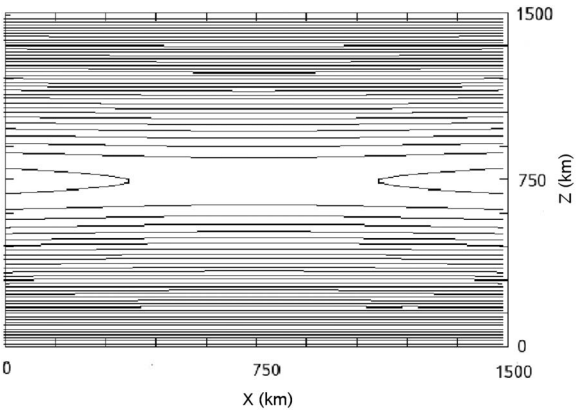

FIG. 12. Evolution for the magnetic field lines in the magnetic reconnection process at $t=7500\delta t$.

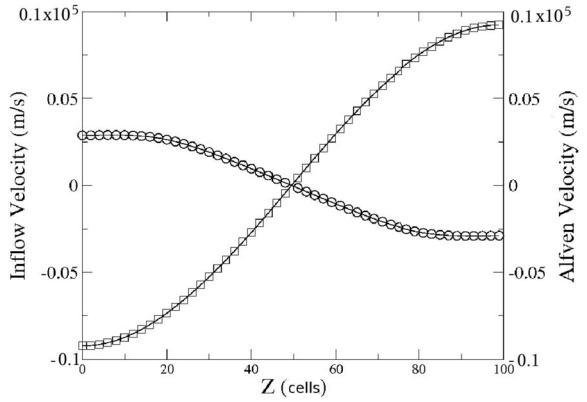

FIG. 13. Inflow velocity (circle) and Alfvén velocity (square) vs z at $t=2500\delta t$ and $x=0$.

V. CONCLUSION

In this paper we introduce a 3D lattice Boltzmann for plasmas, which is able to simulate magnetic reconnection without any previous assumption of a resistive region or an anomalous resistivity. The model simulates the plasma as two fluids (one electronic and one ionic) with an interaction term. It reproduces in the continuous limit the equations of the two-fluids theory and, therefore, the MHD Hall equations. This model can simulate either conducting and viscous fluids in the incompressible limit or nonviscous compressible fluids, and successfully reproduces both the Hartmann flow and the magnetic reconnection in the magnetotail. The local reconnection rates we obtain for the magnetotail with this model are between $R=0.062$ and $R=0.073$, which is in good agreement with observations.

Since this method includes both electric and magnetic fields, plus the density and velocity fields for each fluid, it gives much more insight on the details of plasma physics. Moreover, it opens the door to much more sophisticated boundary conditions, such as conductive walls or electromagnetic waves in plasmas. This is an advantage upon other magnetohydrodynamic LB models. Furthermore, it is 3D, so many interest phenomena can be investigated here. The model does not require large computational resorces. It just takes between 6 h and 7 h in a Pentium IV PC of 3.0 GHz and uses around 13 MB of RAM.

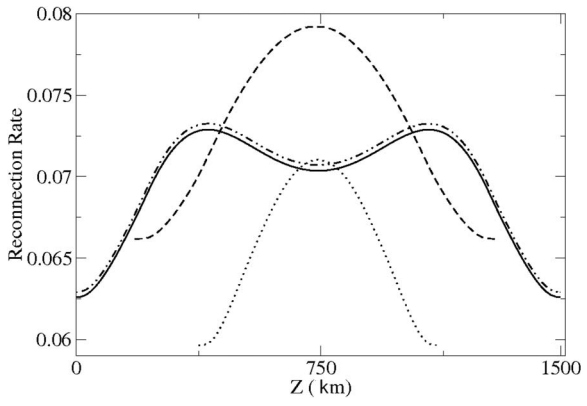

FIG. 14. Reconnection rate vs z at $t=2500\delta t$ and $x=0$. The following curves were computed with $\delta x=15$ km: the dotted line is for a simulation zone of 750×750 km, the dashed line is for a simulation zone of 1125×1125 km, and the solid line is for a simulation zone of 1500×1500 km. In addition, the dotted-dotted-dashed line is obtained for the same simulation zone of the solid line (1500×1500 km) with $\delta x=7.5$ km.

As other methods do, the stability of our model is related with the electron to ion mass ratio. Systematic errors cumulate with time, and finally the model becomes unstable. The stabilization time falls down with larger mass ratios. The simulation for the magnetic reconnection rate in the magnetotail we shown above is almost at the limit of good performance, but it is remarkable that the model reaches enough stability to see reliable results with the actual mass ratio of $m_i/m_e=1820$ that can be compared with experimental results. We also ran simulations with mass ratios of $m_i/m_e=20$ and $m_i/m_e=100$, which were much more stable. Other LB models for magnetohydrodynamics [6–13] and two fluids (usual fluid dynamics, not plasmas) exhibit unstabilities when they consider mass ratios larger than 10. In these models, the automaton velocity is similar to the speed of sound. In contrast, the automaton velocity for our model is a little bit larger than the speed of light (actually, it is $\sqrt{2}c$), and the time steps are, thus, much shorter. This is for us the most reliable source of stability in our model.

By investigating the magnetic reconnection in the magnetotail with our lattice Boltzmann model we found a very interesting result. The range and the peak values of the local reconnection rate we have defined by dividing the inflow velocity at each z coordinate by the local Alfven velocity there seems are less affected by the borders in the simulation space than the asymptotic limits for those quantities. Therefore, it seems to be a reliable quantity for the study of magnetic reconnection with models that do not include an explicit diffusive region.

The model introduces the forces at first order in time, but it works properly for weak electromagnetic fields and low resistive plasmas, including the magnetotail values. These limits depend on the electron and ion mass ratio. When this ratio is small, it is able to work with stronger electromagnetic field and larger time steps, but this modifies the MHD Hall equation; however, such small ratios have been widely used in the simulation of magnetic reconnection processes, without large precision loses [24].

If the mass ratio is set to one, the model reproduces resistive MHD. Small deviations from this unity ratio allows for a tuning of the Hall terms in the generalized Ohm's law. This would allow one to simulate other phenomena, such as the magnetic reconnection in the solar flares. Moreover, since the model reproduces all terms of the generalized Ohm's law, even plasmas with significative strong oscillations of the electric field could also be simulated, as it is the case of many plasmas in the laboratory. Since it is a two-fluid model, it may be possible to simulate such processes where ions and electrons separate smoothly from each other, as in the ionosphere. In addition, because this model also reproduces the Maxwell equations, it can also be used to reproduce the Faraday rotation of the polarization plain of electromagnetic waves crossing astrophysical plasmas. It seems also possible to develop models including forces at second order in time,

or LB models with 13 velocity vectors for the fluids, as proposed by [27]. All these are promisory paths of future work.

Summarizing, we have introduced a 3D lattice Boltzmann model that reproduces the two-fluid theory for plasmas and includes in a natural way many aspects of interest in plasma physics, such as electric fields and magnetic reconnection. It has been shown in this work that this model can actually be used to investigate real astrophysical problems, but it seems to be able to cover a much broader range of applications. We hope that this LB model will contribute to the study of plasma physics in many interesting phenomena.

ACKNOWLEDGMENTS

The authors are thankful to Dominique d'Humières for his interest and his papers on the method of lattice Boltzmann. We also thank the National University of Colombia for financial support and an anonymous referee for his suggestions and corrections.

APPENDIX: CHAPMAN-ENSKOG EXPANSION

The Boltzmann equations for each fluid, Eqs. (8)–(11), determine the system evolution. This evolution rule gives in the continuum limit the macroscopic differential equations that the system satisfies. This is known as the Chapman-Enskog expansion. To develop it, we start by taking the Taylor expansion of these equations until second order in spatial and temporal variables,

$$\vec{v}_i^p \cdot \vec{\nabla} f_i^{p(s)} + \frac{1}{2}\sum_{\alpha,\beta} \frac{\partial^2 f_i^{p(s)}}{\partial x_\alpha \partial x_\beta}(v_{i\alpha}^p v_{i\beta}^p) + \frac{\partial f_i^{p(s)}}{\partial t} + \frac{\partial}{\partial t}\vec{v}_i^p \cdot \vec{\nabla} f_i^{p(s)} + \frac{1}{2}\frac{\partial^2 f_i^{p(s)}}{\partial t^2} = -\frac{1}{\tau_s}(f_i^{p(s)} - f_i^{p(s)\mathrm{eq}}) + T_i^{(s)}, \tag{A1}$$

$$\vec{v}_i^p \cdot \vec{\nabla} G_{ij}^p + \frac{1}{2}\sum_{\alpha,\beta} \frac{\partial^2 G_{ij}^p}{\partial x_\alpha \partial x_\beta}(v_{i\alpha}^p v_{i\beta}^p) + \frac{\partial G_{ij}^p}{\partial t} + \frac{\partial}{\partial t}\vec{v}_i^p \cdot \vec{\nabla} G_{ij}^p + \frac{1}{2}\frac{\partial^2 G_{ij}^p}{\partial t^2}\delta t^2 = -\frac{1}{\tau_2}(G_{ij}^p - G_{ij}^{p\,\mathrm{eq}}), \tag{A2}$$

$$\frac{\partial f_0^{(s)}}{\partial t} + \frac{1}{2}\frac{\partial^2 f_0^{(s)}}{\partial t^2} = -\frac{1}{\tau_s}(f_0^{(s)} - f_0^{(s)\mathrm{eq}}) + T_0^{(s)}, \tag{A3}$$

$$\frac{\partial G_0}{\partial t} + \frac{1}{2}\frac{\partial^2 G_0}{\partial t^2} = -\frac{1}{\tau_2}(G_0 - G_0^{\mathrm{eq}}). \tag{A4}$$

where $\alpha,\beta = x,y,z$ denotes the components in the x, y, and z directions.

Next, we expand the distribution functions and the spatial and time derivatives in a power series on a small parameter, ϵ,

$$G_{ij}^p = G_{ij}^{p(0)} + \epsilon G_{ij}^{p(1)} + \epsilon^2 G_{ij}^{p(2)} + \cdots, \tag{A5}$$

$$f_i^{p(s)} = f_i^{p(s)(0)} + \epsilon f_i^{(s)(1)} + \epsilon^2 f_i^{p(s)(2)} + \cdots, \tag{A6}$$

$$\frac{\partial}{\partial t} = \epsilon\frac{\partial}{\partial t_1} + \epsilon^2\frac{\partial}{\partial t_2} + \cdots, \tag{A7}$$

$$\frac{\partial}{\partial x_\alpha} = \epsilon\frac{\partial}{\partial x_{\alpha 1}} + \cdots. \tag{A8}$$

It is assumed that only the zero order terms in ϵ of the distribution functions contribute to the macroscopic variables. So, for $n>0$ we have

$$f_0^{s(n)} + \sum_{i,p} f_i^{p(s)(n)} = 0, \tag{A9a}$$

$$\sum_{i,p} f_i^{p(s)(n)}\vec{v}_i^p = 0, \tag{A9b}$$

$$\sum_{i,j,p} G_{ij}^{p(n)}\vec{e}_{ij}^p = 0, \tag{A9c}$$

$$\sum_{i,j,p} G_{ij}^{p(n)}\vec{b}_{ij}^p = 0. \tag{A9d}$$

The external forces $\vec{F}^{(s)}$ and the mean current density $\vec{J}'$ are of order ϵ [15], so we can write $\vec{F}^{(s)} = \epsilon\vec{F}_1^{(s)}$, $\vec{J}' = \epsilon\vec{J}'_1$, $T_i^{(s)} = \epsilon T_{1i}^{(s)}$, and $T_0^{(s)} = \epsilon T_{10}^{(s)}$. Because $f_i^{p(s)\mathrm{eq}}$ and $G_{ij}^{p\mathrm{eq}}$ are now functions of $\vec{F}^{(s)}$ and $\vec{J}'$, we need to develop a Chapman-Enskog expansion of the equilibrium function, too,

$$f_i^{p(s)\mathrm{eq}} = f_i^{p(s)(0)\mathrm{eq}} + \epsilon f_i^{p(s)(1)\mathrm{eq}} + \epsilon^2 f_i^{p(s)(2)\mathrm{eq}}, \tag{A10}$$

$$G_{ij}^{p\mathrm{eq}} = G_{ij}^{p(0)\mathrm{eq}} + \epsilon G_{ij}^{p(1)\mathrm{eq}} + \epsilon^2 G_{ij}^{p(2)\mathrm{eq}}. \tag{A11}$$

Thus, by replacing these results into Eqs. (A1)–(A4), we obtain at zeroth order of ϵ

$$f_i^{p(s)(0)\mathrm{eq}} = f_i^{p(s)(0)}, \tag{A12a}$$

$$f_0^{(s)(0)\mathrm{eq}} = f_0^{(s)(0)}, \tag{A12b}$$

$$G_{ij}^{p(0)\mathrm{eq}} = G_{ij}^{p(0)}. \tag{A12c}$$

$$G_0^{\mathrm{eq}} = G_0^{(0)}. \tag{A12d}$$

For the first-order terms in ϵ of the distribution functions we obtain

$$\vec{v}_i^p \cdot \vec{\nabla}_1 f_i^{p(s)(0)} + \frac{\partial f_i^{p(s)(0)}}{\partial t_1} = -\frac{1}{\tau_s}(f_i^{p(s)(1)} - f_i^{p(s)(1)\mathrm{eq}}) + T_{1i}^{(s)}, \tag{A13a}$$

$$\vec{v}_i^p \cdot \vec{\nabla}_1 G_{ij}^{p(0)} + \frac{\partial G_{ij}^{p(0)}}{\partial t_1} = -\frac{1}{\tau_2}(G_{ij}^{p(1)} - G_{ij}^{p(1)\mathrm{eq}}), \tag{A13b}$$

$$\frac{\partial f_0^{(s)(0)}}{\partial t_1} = -\frac{1}{\tau_s}(f_0^{(s)(1)} - f_0^{(s)(1)\mathrm{eq}}) + T_{10}^{(s)}, \tag{A13c}$$

$$\frac{\partial G_0^{(0)}}{\partial t_1} = -\frac{1}{\tau_2}(G_0^{(1)} - G_0^{(1)\mathrm{eq}}), \tag{A13d}$$

and for the second-order terms in ϵ we have

$$\left(1-\frac{1}{2\tau_s}\right)\left(\vec{v}_i^p\cdot\vec{\nabla}_1+\frac{\partial}{\partial t_1}\right)f_i^{p(s)(1)}+\frac{\partial f_i^{p(s)(0)}}{\partial t_2}+\frac{1}{2\tau_s}\left(\vec{v}_i^p\cdot\vec{\nabla}_1+\frac{\partial}{\partial t_1}\right)f_i^{p(s)(1)\mathrm{eq}}+\frac{1}{2}\left(\vec{v}_i^p\cdot\vec{\nabla}_1+\frac{\partial}{\partial t_1}\right)T_{1i}^{(s)} = -\frac{1}{\tau_s}(f_i^{p(s)(2)}-f_i^{p(s)(2)\mathrm{eq}}), \tag{A14a}$$

$$\left(1-\frac{1}{2\tau_2}\right)\left(\vec{v}_i^p\cdot\vec{\nabla}_1+\frac{\partial}{\partial t_1}\right)G_{ij}^{p(1)}+\frac{\partial G_{ij}^{p(0)}}{\partial t_2}+\frac{1}{2\tau_2}\left(\vec{v}_i^p\cdot\vec{\nabla}_1+\frac{\partial}{\partial t_1}\right)G_{ij}^{p(1)\mathrm{eq}} = -\frac{1}{\tau_2}(G_{ij}^{p(2)}-G_{ij}^{p(2)\mathrm{eq}}), \tag{A14b}$$

$$\left(1-\frac{1}{2\tau_s}\right)\frac{\partial f_0^{(s)(1)}}{\partial t_1}+\frac{\partial f_0^{(s)(0)}}{\partial t_2}+\frac{1}{2\tau_s}\frac{\partial f_0^{(s)(1)\mathrm{eq}}}{\partial t_1}+\frac{1}{2}\frac{\partial T_{10}^{(s)}}{\partial t_1} = -\frac{1}{\tau_s}(f_0^{(s)(2)}-f_0^{(s)(2)\mathrm{eq}}), \tag{A14c}$$

$$\left(1-\frac{1}{2\tau_2}\right)\frac{\partial G_0^{(1)}}{\partial t_1}+\frac{\partial G_0^{(0)}}{\partial t_2}+\frac{1}{2\tau_2}\frac{\partial G_0^{(1)\mathrm{eq}}}{\partial t_1} = -\frac{1}{\tau_2}(G_0^{(2)}-G_0^{(2)\mathrm{eq}}). \tag{A14d}$$

The terms of order one and two for the equilibrium functions of the fluids are obtained by replacing Eq. (16) into Eq. (21). That gives

$$f_i^{p(s)\mathrm{eq}}(\vec{x},t) = \omega_i\rho_s\left\{3\xi_s\rho_s^{\gamma-1}+3\left[\vec{v}_i^p\cdot\left(\vec{V}_s+\frac{\epsilon\vec{F}_1^{(s)}}{2\rho_s}\right)\right]+\frac{9}{2}\left[\vec{v}_i^p\cdot\left(\vec{V}_s+\frac{\epsilon\vec{F}_1^{(s)}}{2\rho_s}\right)\right]^2-\frac{3}{2}\left(\vec{V}_s+\frac{\epsilon\vec{F}_1^{(s)}}{2\rho_s}\right)^2\right\}, \tag{A15a}$$

$$f_0^{p(s)\mathrm{eq}}(\vec{x},t) = 3\rho_s\left\{1-\frac{1}{2}\left[4\xi_s\rho_s^{\gamma-1}+\left(\vec{V}_s+\frac{\epsilon\vec{F}_1^{(s)}}{2\rho_s}\right)^2\right]\right\}. \tag{A15b}$$

From these equations we can obtain

$$f_i^{p(s)(0)\mathrm{eq}}(\vec{x},t) = \omega_i\rho_s\left[3\xi_s\rho_s^{\gamma-1}+3(\vec{v}_i^p\cdot\vec{V}_s)+\frac{9}{2}(\vec{v}_i^p\cdot\vec{V}_s)^2-\frac{3}{2}(\vec{V}_s)^2\right], \tag{A16a}$$

$$f_i^{p(s)(1)\mathrm{eq}}(\vec{x},t) = \omega_i\left[\frac{3}{2}(\vec{v}_i^p\cdot\vec{F}_1^{(s)})\right]+\frac{9}{2}(\vec{v}_i^p\cdot\vec{V}_s)(\vec{v}_i^p\cdot\vec{F}_1^{(s)})-\left[\frac{3}{2}(\vec{V}_s\cdot\vec{F}_1^{(s)})\right], \tag{A16b}$$

$$f_i^{p(s)(2)\mathrm{eq}}(\vec{x},t) = \frac{\omega_i}{\rho_s}\left[\frac{9}{4}(\vec{v}_i^p\cdot\vec{F}_1^{(s)})^2\right]\left[-\frac{3}{4}(\vec{F}_1^{(s)})^2\right], \tag{A16c}$$

and

$$f_0^{p(s)(0)\mathrm{eq}}(\vec{x},t) = 3\rho_s\left\{1-\frac{1}{2}[4\xi_s\rho_s^{\gamma-1}+(\vec{V}_s)^2]\right\}, \tag{A16d}$$

$$f_0^{p(s)(1)\mathrm{eq}}(\vec{x},t) = -3\left[\frac{1}{2}(\vec{V}_s\cdot\vec{F}_1^{(s)})\right], \tag{A16e}$$

$$f_0^{p(s)(2)\mathrm{eq}}(\vec{x},t) = -\frac{3}{\rho_s}\left(\frac{1}{4}(\vec{F}_1^{(s)}\cdot\vec{F}_1^{(s)})\right), \tag{A16f}$$

The same process can be used to determine the terms of order 1 and 2 for the equilibrium functions of the electromagnetic fields. Replacing Eq. (14) into Eq. (24) and grouping, we have

$$G_{ij}^{p(0)\mathrm{eq}}(\vec{x},t) = \frac{1}{4}\vec{E}\cdot e_{ij}^p+\frac{1}{8}\vec{B}\cdot b_{ij}^p, \tag{A17a}$$

$$G_{ij}^{p(1)\mathrm{eq}}(\vec{x},t) = -\frac{\epsilon\mu_0}{16}\vec{J'}_1\cdot e_{ij}^p, \tag{A17b}$$

$$G_{ij}^{p(2)\mathrm{eq}}(\vec{x},t) = 0. \tag{A17c}$$

Now, we are ready to determine the equation that the model satisfies in the continuum limit. First, let us consider nonviscous compressible fluids, that is $\tau_s=\frac{1}{2}$. By summing up Eq. (A13a) over i and p, and by taking into account Eqs. (A13c), (7), (A16), and (A9), we obtain

$$\vec{\nabla}\cdot(\rho_s\vec{V}_s)+\frac{\partial\rho_s}{\partial t_1} = 0. \tag{A18}$$

By summing up Eq. (A14a) in the same way, we obtain

$$\vec{\nabla}\cdot\left(\frac{1}{2}\vec{F}_1^{(s)}\right)+\frac{\partial\rho_s}{\partial t_2} = 0. \tag{A19}$$

Now, we can add these two equations to obtain

$$\vec{\nabla}\cdot\left(\rho_s\vec{V}_s+\frac{1}{2}\vec{F}_1^{(s)}\right)+\frac{\partial\rho_s}{\partial t_1} = 0. \tag{A20}$$

Next, following Guo *et al.*, [15], and by taking into account Eq. (16), we arrive to the continuity equation

$$\vec{\nabla}\cdot(\rho_s\vec{V}_s')+\frac{\partial\rho_s}{\partial t} = 0. \tag{A21}$$

By multiplying Eq. (A13a) by $\vec{v}_i^p$ and summing up over i and p, we obtain

$$\frac{\partial}{\partial x_\beta}(\rho_s V_{s\alpha}V_{s\beta})+\frac{\partial(\xi_s\rho_s^\gamma)}{\partial x_\alpha}+\frac{\partial(\rho_s V_{s\alpha})}{\partial t_1} = F_{1\alpha}^{(s)}. \tag{A22}$$

In a similar way, by multiplying Eq. (A14a) by $\vec{v}_i^p$ and summing up over i and p, we obtain

$$\frac{\partial(\rho_s V_{s\alpha})}{\partial t_2} + \frac{1}{2}\frac{\partial}{\partial x_\beta}(F^{(s)}_{1\beta} V_{s\alpha} + F^{(s)}_{1\alpha} V_{s\beta}) + \frac{1}{2}\frac{\partial F^{(s)}_{1\alpha}}{\partial t_1} = 0. \tag{A23}$$

Now, we can add these two equations and replace Eq. (16) to obtain (up to second order in ϵ)

$$\frac{\partial(\rho_s V'_{s\alpha})}{\partial t} + \frac{\partial}{\partial x_\beta}(\rho_s V'_{s\alpha} V'_{s\beta}) = -\frac{\partial P_s}{\partial x_\alpha} + F^{(s)}_{1\alpha}. \tag{A24}$$

This is the Navier-Stokes equation for nonviscous compressible fluids. In our model, the force $F^{(s)}_\alpha$ is taken at first order in ϵ. With this approximation, Eq. (13) gives $F^{(s)}_{1\alpha}(\vec{V}_s) = F^{(s)}_{1\alpha} \times (\vec{V}'_s)$, and the Navier-Stokes equation is

$$\frac{\partial(\rho_s V'_{s\alpha})}{\partial t} + \frac{\partial}{\partial x_\beta}(\rho_s V'_{s\alpha} V'_{s\beta}) = -\frac{\partial P_s}{\partial x_\alpha} + \left(\frac{q_s}{m_s}\rho_s(\vec{E}' + \vec{V}'_s \times \vec{B}) - \nu\rho_s(\vec{V}'_s - \vec{V}'_{(s+1) \bmod 2})\right)_\alpha + F_{0\alpha}. \tag{A25}$$

By replacing Eq. (A21) into Eq. (A25), we arrive at the usual form of the Navier-Stokes equation for a nonviscous compressible fluid [4]

$$\rho_s\left(\frac{\partial \vec{V}'_s}{\partial t} + (\vec{V}' \cdot \vec{\nabla})\vec{V}'_s\right) = -\vec{\nabla}P_s + \frac{q_s}{m_s}\rho_s(\vec{E}' + \vec{V}'_s \times \vec{B}) - \nu\rho_s(\vec{V}'_s - \vec{V}'_{(s+1) \bmod 2}) + \vec{F}_0. \tag{A26}$$

Second, let us consider both fluids with viscosity ($\tau_s > 1/2$) in the incompressible limit. By following the same procedure, we arrive to the following momentum equation (up to second order in ϵ):

$$\frac{\partial(\rho_s V'_{s\alpha})}{\partial t} + \frac{\partial}{\partial x_\beta}(\rho_s V'_{s\alpha} V'_{s\beta}) = -\frac{\partial P_s}{\partial x_\alpha} + \left(\frac{q_s}{m_s}\rho_s(\vec{E}' + \vec{V}'_s \times \vec{B}) - \nu\rho_s(\vec{V}'_s - \vec{V}'_{(s+1) \bmod 2})\right)_\alpha + \eta_s\rho_s\vec{\nabla}^2 V'_{s\alpha} + F_{0\alpha}, \tag{A27}$$

where the kinematic viscosity is $\eta_s = \frac{1}{3}(\tau_s - 1/2)$. By following the same procedure described above [4], we obtain

$$\rho_s\left(\frac{\partial \vec{V}'_s}{\partial t} + (\vec{V}' \cdot \vec{\nabla})\vec{V}'_s\right) = -\vec{\nabla}P_s + \frac{q_s}{m_s}\rho_s(\vec{E}' + \vec{V}'_s \times \vec{B}) - \nu\rho_s(\vec{V}'_s - \vec{V}'_{(s+1) \bmod 2}) + \vec{F}_0 + \eta_s\rho_s\vec{\nabla}^2\vec{V}'_s. \tag{A28}$$

The energy evolution equation is not necessary because it is obtained by replacing Eq. (27) into Eq. (A21), that is

$$\vec{\nabla} \cdot \left[\left(\frac{P_s}{\xi_s}\right)^{1/\gamma}\vec{V}'_s\right] + \frac{\partial}{\partial t}\left(\frac{P_s}{\xi_s}\right)^{1/\gamma} = 0, \tag{A29}$$

so that

$$\frac{P_s^{1/\gamma-1}}{\gamma\xi_s^{1/\gamma}}\vec{V}'_s \cdot \nabla P_s + \left(\frac{P_s}{\xi_s}\right)^{1/\gamma}\vec{\nabla} \cdot \vec{V}'_s + \frac{P_s^{1/\gamma-1}}{\gamma\xi_s^{1/\gamma}}\frac{\partial P_s}{\partial t} = 0, \tag{A30}$$

that can be simplified to obtain

$$\frac{\partial P_s}{\partial t} + \vec{V}'_s \cdot \nabla P_s + \gamma P_s\vec{\nabla} \cdot \vec{V}'_s = 0. \tag{A31}$$

For the electromagnetic field, we take $\tau_2 = 1/2$. By summing up Eqs. (A13b), (A13d), (A14b), and (A14d) on i, j, and p, we do not obtain any information about the fields. Thus, let us multiply these equations by $\vec{e}^p_{ij}$ before summing up. That gives

$$\frac{\partial \vec{E}}{\partial t_1} - \frac{1}{2}\vec{\nabla} \times \vec{B} = -\frac{1}{2}\mu_0 \vec{J}'_1, \tag{A32}$$

and

$$\frac{\partial \vec{E}}{\partial t_2} - \frac{\mu_0}{4}\frac{\partial \vec{J}'_1}{\partial t_1} = 0. \tag{A33}$$

If we add these two equations, and because of Eq. (14), we obtain the first Maxwell equation,

$$\frac{\partial \vec{E}'}{\partial t} - \frac{1}{2}\vec{\nabla} \times \vec{B} = -\mu_0\frac{1}{2}\vec{J}'. \tag{A34}$$

Similarly, multiplying Eqs. (A13b) and (A14b) by $\vec{b}^p_{ij}$ and summing up on i, j, and p gives

$$\frac{\partial \vec{B}}{\partial t_1} + \vec{\nabla} \times \vec{E} = 0 \tag{A35}$$

and

$$\frac{\partial \vec{B}}{\partial t_2} - \frac{1}{2}\vec{\nabla} \times \left(\frac{1}{2}\mu_0 \vec{J}'_1\right) = 0. \tag{A36}$$

If we add these two last equations, we obtain the second Maxwell equation,

$$\frac{\partial \vec{B}}{\partial t} + \vec{\nabla} \times \vec{E}' = 0. \tag{A37}$$

The other two Maxwell equations can be obtained from the Eqs. (A34) and (A37) as follows [4]. If one applies the divergence to these equations we obtain

$$\frac{\partial(\vec{\nabla} \cdot \vec{E}')}{\partial t} = -\frac{1}{2}\mu_0\vec{\nabla} \cdot \vec{J}', \tag{A38}$$

$$\frac{\partial(\vec{\nabla} \cdot \vec{B})}{\partial t} = 0. \tag{A39}$$

Now, let us replace Eq. (15) in Eq. (A38) to obtain

$$\frac{\partial(\vec{\nabla}\cdot\vec{E}')}{\partial t} = -\frac{1}{2}\mu_0\left(\frac{q_0}{m_0}\vec{\nabla}\cdot(\rho_0\vec{V}'_0) + \frac{q_1}{m_1}\vec{\nabla}\cdot(\rho_1\vec{V}'_1)\right), \tag{A40}$$

and because of the two fluids satisfy the continuity equations (A21) we obtain

$$\frac{\partial(\vec{\nabla}\cdot\vec{E}')}{\partial t} = \frac{1}{2}\mu_0\left(\frac{q_0}{m_0}\frac{\partial\rho_0}{\partial t} + \frac{q_1}{m_1}\frac{\partial\rho_1}{\partial t}\right). \tag{A41}$$

By taking into account Eq. (7), we finally obtain

$$\frac{\partial\left(\vec{\nabla}\cdot\vec{E}' - \frac{1}{2}\mu_0\rho_c\right)}{\partial t} = 0. \tag{A42}$$

Thus, if the initial conditions for the electromagnetic fields satisfy the Maxwell equations

$$\vec{\nabla}\cdot\vec{B} = 0. \tag{A43}$$

$$\vec{\nabla}\cdot\vec{E}' = \frac{1}{2}\mu_0\rho_c = \frac{\rho_c}{\epsilon_0}. \tag{A44}$$

This equations will be recovered for all times.

Summarizing, the adiabatic state equation, Eq. (27), and Eqs. (A21) and (A25) determine the behavior of a nonviscous compressible plasma. If we use Eq. (A27) instead of Eq. (A25), the model reproduces the behavior of an incompressible plasma with viscosity. Equations (A34), (A37), (A43), and (A44), that is, the maxwell equations, determine the evolution of the electromagnetic fields. These are the equations of the two-fluids theory [4] and this completes the proof.

[1] E. N. Parker, Proc. IAU Symp. **6**, 123 (1958).
[2] E. N. Parker, Phys. Rev. **107**, 830 (1957).
[3] H. E. Petschek, in AAS/NASA Symposium on The Physics of Solar Flares, edited by W. N. Hess (Aeronautics and Space Administration, Washington, D.C., 1964), p. 425.
[4] Introduction to plasma physics i, fall 2003, http://ocw.mit.edu/OcwWeb/Physics/index.htm
[5] G. R. McNamara and G. Zanetti, Phys. Rev. Lett. **61**, 2332 (1988).
[6] S. Chen, H. Chen, D. Martinez, and W. Matthaeus, Phys. Rev. Lett. **67**, 3776 (1991).
[7] S. Chen, D. O. Martinez, W. H. Matthaeus, and H. Chen, J. Stat. Phys. **68**, 533 (1992).
[8] H. Chen and W. H. Matthaeus, Phys. Rev. Lett. **58**, 1845 (1987).
[9] H. Chen, W. H. Matthaeus, and L. W. Klein, Phys. Fluids **31**, 1439 (1988).
[10] D. O. Martinez, S. Chen, and W. H. Matthaeus, Phys. Plasmas **1**, 1850 (1994).
[11] B. R. Osborn, Master thesis, University of Maryland, 2004.
[12] G. Breyiannis and D. Valougeorgis, Phys. Rev. E **69**, 065702(R) (2004).
[13] G. Fogaccia, R. Benzi, and F. Romanelli, Phys. Rev. E **54**, 4384 (1996).
[14] P. Bathnagar, E. Gross, and M. Krook, Phys. Rev. **94**, 511 (1954).
[15] Z. Guo, C. Zheng, and B. Shi, Phys. Rev. E **65**, 046308 (2002).
[16] W. Schaffenberger and A. Hanslmeier, Phys. Rev. E **66**, 046702 (2002).
[17] J. J. David, *Electrodinámica clásica*, 1st ed. (Editorial Alhambra, S.A., Madrid, 1966).
[18] E. G. Harris, Nuovo Cimento **23**, 115 (1962).
[19] B. J. R. Sommer and K. Schindler, Astrophys. Space Sci. **35**, 389 (1975).
[20] P. L. Pritchett and F. Coroniti, Earth, Planets Space **53**, 635 (2001).
[21] B. Lembège and R. Pellat, Phys. Fluids **25**, 1995 (1982).
[22] A. Runov *et al.*, Ann. Geophys. **23**, 1391 (2005).
[23] A. Runov, V. Sergeev, R. Nakamura, W. Baumjohann, T. L. Zhang, Y. Asano, M. Volwerk, Z. Voros, A. Balogh, and H. Rème, Planet. Space Sci. **53**, 237 (2005).
[24] M. Hesse, K. Schindler, J. Birn, and M. Kuznetsova, Phys. Plasmas **6**, 1781 (1999).
[25] Y. Asano, T. Mukai, M. Hoshino, Y. Saito, H. Hayakawa, and T. Nagai, J. Geophys. Res. **109**, A02212 (2004).
[26] C. Xiao *et al.*, in Proceedings of Cluster and Double Star Symposium—5th Anniversary of Cluster in Space, Noordwijk, The Netherlands, 2005 (ESA Publ. Div., Noordwijk, 2006).
[27] T. Cowling, *Magnetohydrodynamic*, 4th ed. (Interscience Publishers, New York, 1968).